GROWTH AND CHARACTERISATION OF SPRAY PYROLYTIC DOPED ZINC AND ALUMINIUM OXIDES SPECTRAL SELECTIVE THIN FILMS.

P.N. Njingana, K.G. Chinyama, E.L. Meyer and R.T. Taziwa

e-mail:pnjingana@ufh.ac.za

Fort Hare Institute of Technology, University of Fort Hare, P/B X1314, Alice 5700, South Africa

Centre for Renewable and Sustainable Energy Studies

Abstract

Doped zinc and aluminium oxides thin films have been produced by spray pyrolysis process onto standard microscope glass slides at different substrate temperature and for different solution concentrations and spray times. The temperature in the reaction chamber was monitored using a calibrated nickel-chromium thermocouple connected to a multimeter as the output device. Single, double and triple layers were grown in a process that sought to optimize the film properties and tailor them for applications in efficient solar energy structures. Characterization for solid film parameters was successfully conducted on the samples. Optical, electrical and structural properties were determined both experimentally and theoretically. An average solar transmittance of 88 per cent was obtained for doped zinc oxide and 71.9 for aluminium oxide films. Reflectance values in the solar spectrum remained below 20 per cent with minimal absorption except for slightly thicker aluminium oxide coatings. In the infrared region, reflectance peaks were observed in the wavelength range 8,000-13,000 nm. Wavelength dependent refractive index of the coatings were then determined from reflectance and transmittance measurements using the Bruggeman and Maxwell-Garnett effective medium theories. The refractive index was 1.28 for zinc oxide.

Key words: spectral selective, spray pyrolysis, thin solid film, characterization

1. Introduction

Recent years have seen the importance of energy being brought into sharp focus as world economies continue to grow amidst spiraling international prices for conventional sources of energy such as petroleum, coal and hydro electricity. Despite the 2008-2009 world economic meltdown, the demand for energy still ranks high, thus creating a general sense of energy crisis. To mitigate the crisis, there is need to incorporate clean and less costly renewable sources of energy of which solar has the most modest potential among the other renewable forms of energy.

There have been remarkable developments in the utilization of solar by way of solar cells, solar collectors and architectural designs in the recent past. However, the biggest challenge in making solar energy cheaper and reliable lies in the development of effective and efficient solar energy materials for both thermal and photovoltaic applications.

Different materials for thin films have been studied by many researchers for their spectral selectiveness. Indium tin oxide (ITO) has a visible transmission greater than 80 per cent and IR reflectance of about 80 per cent or greater. However, its low availability on the market and the high cost calls for its substitution with other readily available and cheaper materials. Zinc oxide (ZnO) is a II-IV *n*-type semiconductor with large band gap of 3.3 eV at room

temperature. Experimental work has shown that zinc oxide is transparent to most of the solar spectrum and therefore this makes it a good candidate as a transparent conducting oxide and reliably a cheaper replacement for ITO. The common growth methods for ZnO nanostructures include filtered vacuum arc deposition [15], reactive magnetron sputtering [16], pulsed laser deposition and chemical vapour deposition [17].

On the other hand, the aluminium oxide (Al_2O_3) thin films are grown using different techniques that include sputtering, chemical vapour deposition (CVD) and dip-coating techniques.. Thin films of Al_2O_3 have high transparency, chemical stability, electric insulation, heat resistance, large mechanical strength and hardness. The melting point of Al_2O_3 is 2045 ^{o} C, have a high dielectric constant .(9), highly thermodynamically stable, and with high electric field strength and large band gap of 8.8 eV. The Al_2O_3 thin films are applicable as abrading and antireflection coatings and are favourable replacements for SiO_2 gate dielectrics in metal oxide semiconductor (MOS) devices. [10-12].

This undertaking emphasizes on the use a convenient, reliable and cheap spray pyrolysis deposition process to prepare solid thin films and investigate their optical and electrical properties and theoretically model these properties in order to understand their nature and optimize them for applications in efficient solar energy structures.

1.1. Spray Pyrolysis

Spray pyrolysis is one method of chemical vapour film deposition. It is described as a process in which an aqueous solution of metal oxides or halides is dispersed and transported by means of a carrier gas to a suitable substrate where a thin film forms. The process starts with production of small droplets of the precursor solution in the atomizer by way of a carrier gas pumped from a gas cylinder at controlled pressure by a system of pressure gauges.

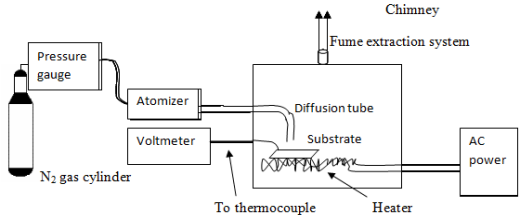

Figure 1. Schematic diagram of the spray pyrolysis unit

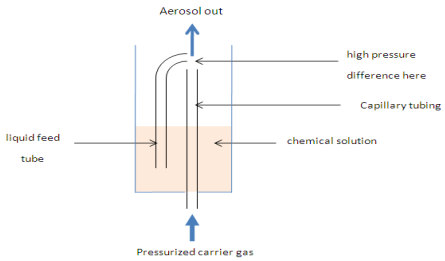

Figure 2. Schematic diagram of the spray pyrolysis atomizer or nebulizer.

These droplets of the spray solution are transported by the carrier gas through a diffusion tube into the reaction chamber and onto a heated substrate where it immediately evaporates leaving a solid thin film. The temperature of the substrate is one of the key parameters that determine the final product and therefore it has to be closely monitored.

2. Experimental Methodology

Zinc nitrate ($ZnCl_{2)}$ doped with a trace of aluminium nitrate hexahydrate ($AlNO_3.6H_2O$) were dissolved in distilled water, forming aqueous solutions of different concentrations and doping levels. A little hydrochloric acid was added to the solution to prevent precipitation to hydroxide. In a similar manner, $AlNO_3.6H_2O$ aqueous solutions doped with zinc were prepared. Using nitrogen as the carrier gas, respective solutions were sprayed through an atomizer or nebulizer onto standard microscope glass substrate slides to form solid thin films. Prior to spraying, the substrates were cleaned in acetone and dried. Different films were obtained for different spray parameters. Optimization of film properties was achieved by varying substrate temperature, solution concentration, carrier gas pressure, doping levels, spray time and multi-laying of films.

Optical characterization in the ultraviolet, visible and infrared (UV/VIS/IR) were conducted using the Perkin Elmer Lambda 19 spectrometer and Perkin Elmer Spectrum BX FT-IR system. Electrical characterization was conducted using a four-point resistance probe whereas the surface and thickness characterization were done using the atomic force microscope and the Tencor Alpha Step profiler respectively.

3. Results and discussion

The temperature in the oven and that of the substrate were monitored with a calibrated chromium-nickel thermocouple. Figure 4 is a calibration curve of the thermocouple. It was also important to know roughly when a required temperature of the substrate is reached after switching the system on. This was achieved by obtaining the oven temperature profile as a function of time. Temperature rise was sharp when the heating elements were just switched on and stabilized steadily as the lapsed time approached the 120 minutes.

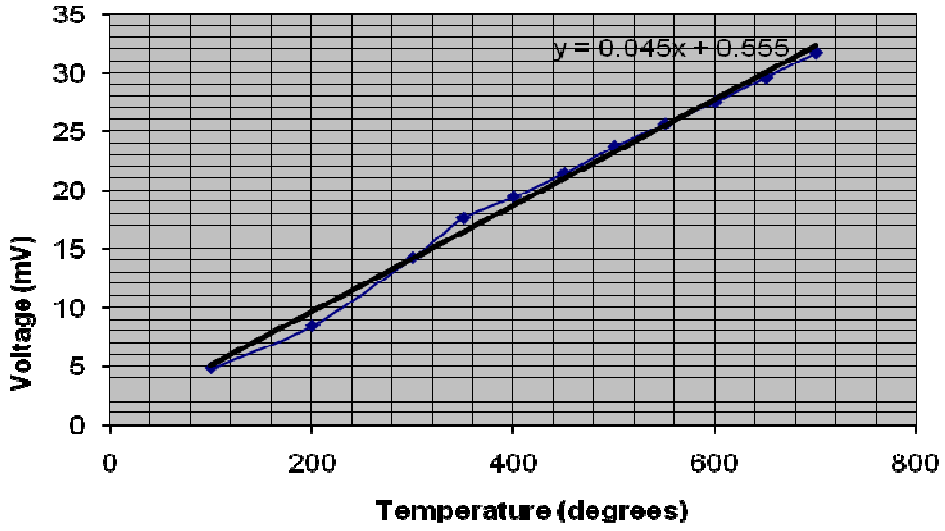

Figure 4. Thermocouple temperature calibration curve.

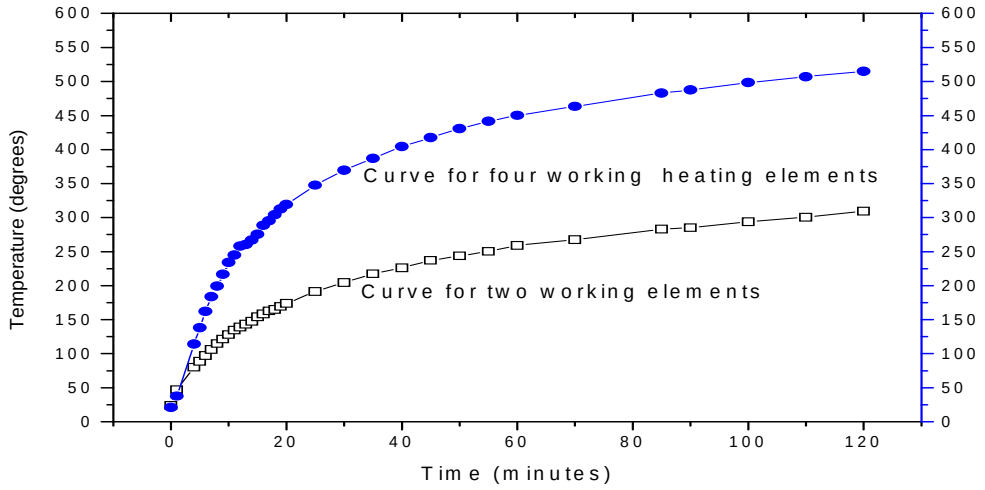

Figure 5. Oven temperature as a function of time.

3.1. Film thickness

Different thicknesses were obtained for films grown using different growth parameters such as spray time, pressure, and concentration of precursor solution and to some extent, substrate temperature. It was observed that more concentrated solutions gave thicker films as compared to less concentrated ones under the same conditions. This is expected because in the former there are more solutes that result into solid film after spraying. The other key parameter that directly affected thickness was spray time. It was observed that longer spray times resulted into thicker films as one would expect. The pressure at which the film was sprayed gave inverse results. The higher the spay pressure the lower the thickness of the film. Logically it would be expected that higher pressure should result into thicker films since more solution would be picked up. While it is true, much of the picked up precursor solution would be sprayed extensively compared to low pressure conditions and in the end what comes to determine the thickness is how long the spray takes. Higher spray pressure also resulted into rapid cooling of the substrate.

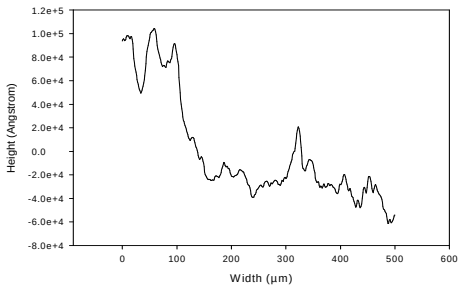

Figure 6. Thickness profile of single layer ZnO thin film.

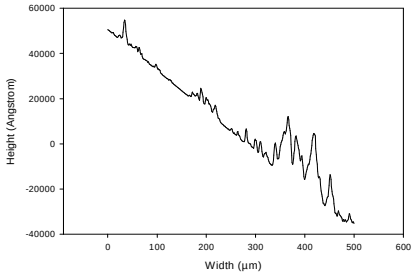

Figure 7. Thickness profile of double a layer aluminium oxide thin film.

The interesting result was that the edges of the thin film resulting from spray pyrolysis tend not to give a step ending but rather steadily reduces in height from the top to the surface of the substrate. Thus in thickness measurements using the step technique, the height of the films were profiled from the top to the bottom, reviewing a slanting curve punctuated by periodic dips suspected to be caused by the stylus' penetration into the film material. The step graph for nearly all the samples had the appearance

similar to the one in the figures above. You will notice a steady slope from the top of the film to the base of the substrate. This implies that in spray pyrolysis process, you obtain non-distinct edges but rather a steady decrease in thickness towards the edge. Thicknesses ranging from 0.14 µm to 87.7 µm have been achieved in this research. It has been noted that time of spray had the greatest influence on the thickness of the resulting coating film.

A UV transmittance cut-off appears to take effect at wavelength near 325 nm and a sharp infrared attenuation was observed at wavelength 2700 nm and at 4100 where the transmittance falls steadily to zero. It has generally been observed that ZnO films allow more of the incidence beam to be transmitted as compared to the aluminium films. The highest transmittance was achieved for ZnO doped with aluminium. The average percent solar transmittance was 88.03 for ZnO and 71.94 for AlO.

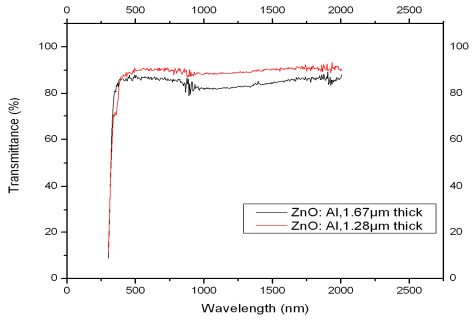

Figure 8. Solar transmittance curves for ZnO: Al films of thicknesses 1.67 μm and 1.28 μm fabricated at 320 ^{o}C and 340 ^{o}C.

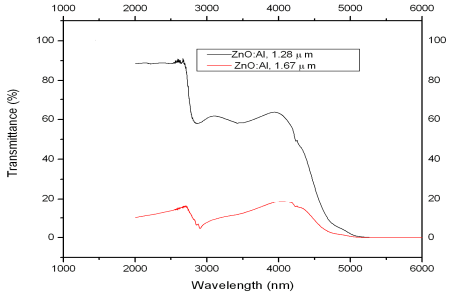

Figure 9. NIR and IR transmittance curves for ZnO:Al films of thicknesses 1.67 μm and 1.28 μm fabricated at 320 ^{o}C and 340 ^{o}C.

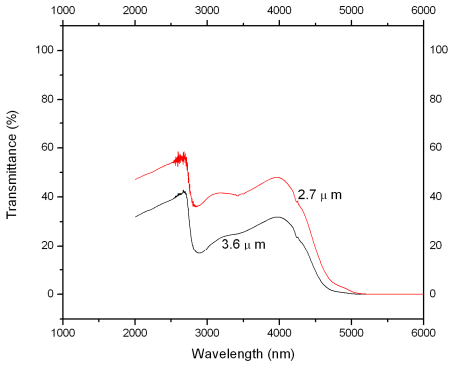

Figure 10. NIR and IR transmittance curves for ZnO:Al films of thicknesses 2.7 μm and 3.6 μm fabricated at 340 ^{o}C and 290 ^{o}C.

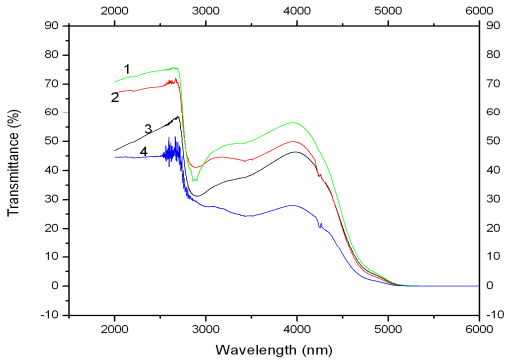

Figure 11. NIR and IR transmittance curves for Al_2O_3 coatings. (1) double layer undoped Al_2O_3 fabricated at 400 ^{o}C, (2) Al_2O_3 : Zn grown at 290 ^{o}C, (3) Al_2O_3 : Zn 400 ^{o}C and (4) Al_2O_3 : Zn 400 ^{o}C.

A similar trend of reflectance values to those of ZnO:Al films were observed in Al_2O_3 coatings as presented in figure 4.4 below. Comparatively, Al_2O_3 has slightly higher reflectance peaks in the same wavelength range.

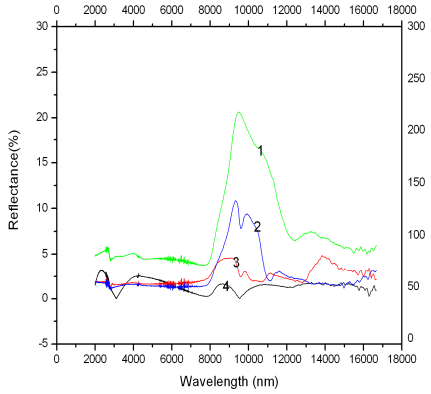

Figure 12. Reflectance curves for ZnO:Al. with different thickness.

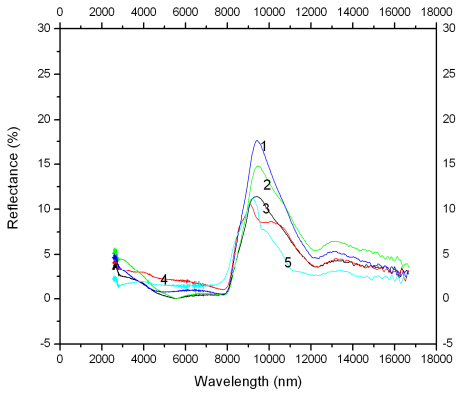

Figure 13. Reflectance curves for Al_2O_3 having different thickness.

In general, it was observed that the reflectance results remained the same in the VIS-NIR spectrum. Therefore, the above graphs are representative of the general trends. However, there is complete reflection of the UV of wavelength below 300 nm.
The analysis with the AFM reviewed interesting structures of the film coatings. The roughness, cross-section and particle analyses were done for samples representing one of the five selected categories. We present here the features of each of the samples with main emphasis being set on surface roughness, surface cross-section and particle size and distribution.

The AFM micrograph presented above reveals the surface structure of the ZnO thin film doped with aluminium. The analysis indicated that the mean roughness for this particular coating was 14.11 nm. In figures 16, one would notice that some sections were deep as presented by the green indicator on the far right of the cross section tracing line. A section indicating some level of deformity is visible in figure 14. The consequence of this is that the thin film tends to have high sheet resistance as a result of those sections that do not have uniform thickness. This deformation gets minimized by way of multi-layer coating, which results in burying the possible discontinuities and improves the thickness uniformity.

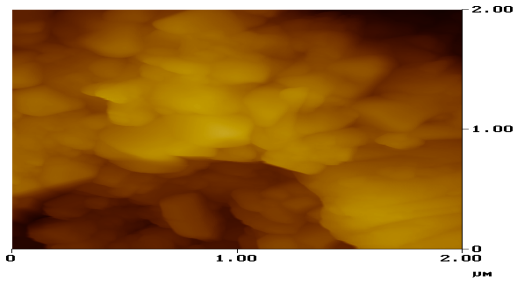

Figure 14. Surface roughness of ZnO doped with aluminium that is 3.6 μm and mean roughness 14.11 nm and grown at 290 ^{o}C.

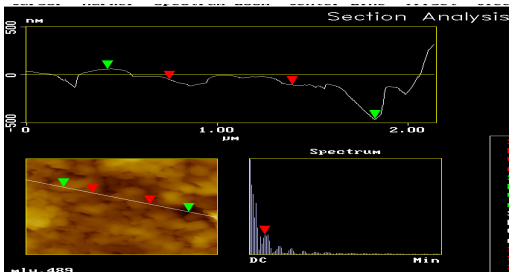

Figure 16. Section analysis of 3.6 μm thick aluminium doped ZnO film deposited at 290 ^{o}C.

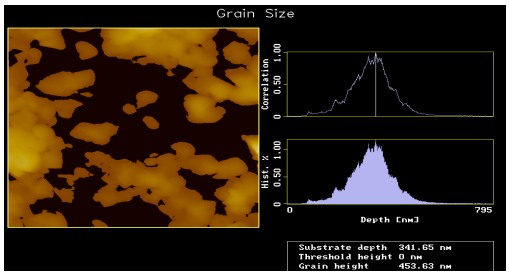

Figure 15. Distribution of grains in the thin film.

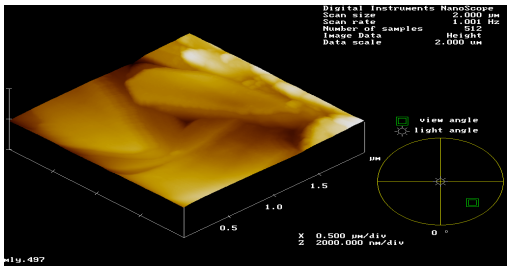

Figure 17. Surface plot of ZnO:Al thin film that is 0.6 μm thick sprayed at 500kPa pressure and 340 ^{o}C substrate temperature.

3.2. Modeling the experimental results

This section examines experimentally derived results and uses them into theoretical models that help us to fully understand these properties and how they fit into the theoretical expectations. The average refractive indices for the two wavelength regions were obtained. Table 1 gives the calculated values in the VIS-NIR-FIR regions.

The resistivities of the film coatings have been calculated. For ZnO:Al the mean values have been found to be 0.29 Ωm whereas for AlO the average value was 0.58 Ωm. These values are on the higher side of most reported values which are of order 10^{-4} Ωm. Reflectance and transmittance values have been used to calculate the absorption coefficients. The result for doped ZnO with thickness 1.2 μm was 662.6 and the highest value rising to 239000. The absorption coefficient has an inversely relation to the thickness of the coating but is also greatly influenced by both transmittance and reflectance values.

SPECTRUM	AVERAGE REFRACTIVE INDEX		
	ZnO	ZnO:Al	Al_2O_3:Zn
VIS-NIR	1.80	1.96	2.00
FIR	1.28	1.53	1.30

Table 1 Wavelength-dependent refractive indices of selected thin films in the VIS/NIR/FIR wavelength regions.

To apply the effective medium theory according to Maxwell-Garnett, we make the assumption that the volumes of the medium constituents are the atoms of the ZnO and Al for the doped samples. We assigned the permeability constants ε_A to aluminium atoms and ε_B to ZnO. The volume of any material is inversely proportional to its density. With this in mind, we took the ratio of densities to represent the volume ratios in the Bruggemann effective medium approximation. Using 1.7< ε_B<2.5 and ε_A= 9 in addition to respective densities of ZnO and aluminium, we got the effective dielectric permeability by applying the following equations:

$$\bar{\varepsilon}^{MG} = \varepsilon_B \left(\frac{\varepsilon_A + 2\varepsilon_B + 2f_A(\varepsilon_A - \varepsilon_B)}{\varepsilon_A + 2\varepsilon_B - f_A(\varepsilon_A - \varepsilon_B)} \right)$$

$$f_A = \frac{a^3}{b^3}$$

This yielded 5< $\bar{\varepsilon}^{MG}$ ≤6.1 as the range of the effective dielectric permeability according to Maxwell-Garnett effective medium approximation. The effect of doping ZnO with aluminium thus increases the effective permeability constant and consequently the refractive index of the film. This further translates to increased refractive index of between 2.2 and 2.4. Application of the Bruggemann effective medium theory required to solve the quadratic equation resulting from the following equation:

$$f_A\left(\frac{\varepsilon_A - \bar{\varepsilon}^{Br}}{\varepsilon_A + 2\bar{\varepsilon}^{Br}}\right) + (1 - f_A)\left(\frac{\varepsilon_B - \bar{\varepsilon}^{Br}}{\varepsilon_B + 2\bar{\varepsilon}^{Br}}\right) = 0$$

The composite medium constituents have been assumed to have equal probability to occupy ε_A for which the valid solutions for the effective dielectric permeability lie between 4.4 and 8.5. The resulting refractive index from this approximation lies between 2.098 and 2.91. Figure 18 gives the graphical representation of the relation between refractive index and reflectance.

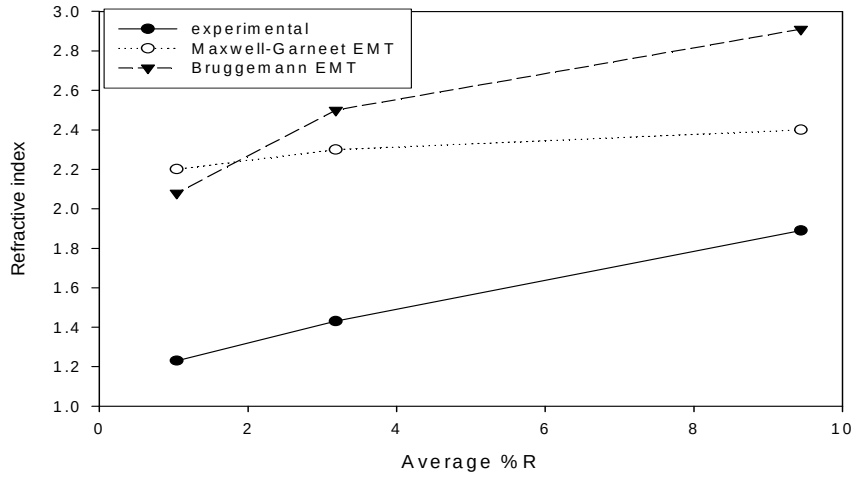

Figure 18 Refractive index as a function of reflectance.

4. Conclusion

This Study has utilized a simple and cheap process of fabricating spectrally selective thin solid films by way of spray pyrolysis process. Process parameters were easy to control with a chance to coat large surfaces. Characterization for solid film parameters was successfully conducted on the samples. Optical and micro-structural properties were determined both experimentally and theoretically. An average solar transmittance of 88 per cent was obtained for doped zinc oxide and 71.9 for aluminium oxide films. In the infrared region, reflectance peaks were observed in the wavelength range 8,000-13,000 nm. Maxwell-Garnett and Bruggemann effective medium theories were applied to obtained effective dielectric permeability of the coatings. The Maxwell-Garnett EMT produced dielectric permeability of 5-6.1 and the Bruggemann approximation yielded 4.4-8.5. These values indicate that doping ZnO with aluminum raises its dielectric permeability and also raises the refractive index.

References

[1] Wontae Cho, K. Sung, K. An, S. S. Lee, C. G. Kim and Y. Kim, KRICT, Daejeon, Korea.

[2] S. Y. Lee, E. S. Shim, H. S. Kang, S. S. Pang, and J. S. Kang, Thin Solid Films, (2005), 437, 31**.**

[3] M. P. Sing, T. Shripathi and S.A Shivashankar, http://www.electrochem.org.

[4] J. Mao, B. Cai, M. Wu and G. Chen, J.Mater.Sci.Tech., **Vol. 19, No. 1**, (2003), pp 368-370.

[5] Hyeong J. Kim, S. Y. No, D. Eom and C. S. Hwang , J.Korean Phy.Soc, **Vol. 49, No. 3**, (2006), pp. 1271_1275.

[6] A.R. Hind and L. Chomette, Varian UV At Work, **No. 090**.

[7] H.J. Möller, (1993), Artech House Inc., London, UK.

[8] T. David, S. Goldsmith and R. L. Boxman, Tel Aviv 69978, Tel Aviv University, Tel Aviv, Israel.

[9] M. Kon, P.K. Song, Y.Shigesato, A. Mizukami and K.Suzuki, Jpn. J.Appl.Phy., **Vol. 41**,(2002), pp 814-819.

[10] K. Krunk, O. Bijakina, V. Mikli, T. Varema and E. Mellikov, Physica Scripta, Vol. T79, (1999), pp 209-212.

[11] S. Berthier and J. Lafait, Optics Communications, Vol. 33, No. 3, (1980), pp 303-306.

[12] S. Brthier, J. Phys. I. France, Vol. 4, (1994), pp 303-318.